Advances in Water Resources 145 (2020) 103740

Contents lists available at ScienceDirect

Advances in Water Resources

journal homepage: www.elsevier.com/locate/advwatres

An approximate analytical solution for non-Darcian flow in a confined aquifer with a single well circulation groundwater heat pump system

Kun Tu[a,b,c,*], Qiang Wu[a,b], Jirka Simunek[c], Ke Zhu[a,b], Chaofan Chen[e,f], Weiyu Zheng[d], Yifan Zeng[a,b], Shengheng Xu[a,b]

[a] College of Geoscience and Surveying Engineering, China University of Mining and Technology, Beijing 100083, China
[b] National Engineering Research Center of Coal Mine Water Hazard Controlling, Beijing 100083, China
[c] Department of Environmental Sciences, University of California, Riverside, CA 92521, USA
[d] School of Energy and Mining Engineering, China University of Mining and Technology, Beijing 100083, China
[e] Helmholtz Centre for Environmental Research (UFZ), Leipzig 04318, Germany
[f] Applied Environmental Systems Analysis, Dresden University of Technology, Dresden 01069, Germany

ARTICLE INFO

Keywords:
Izbash equation
Linearization method
Non-Darcian flow
Geothermal energy
Groundwater heat pump system

ABSTRACT

An analytical model is proposed in this study to describe transient drawdown induced by non-Darcian flow in a confined aquifer with a single well circulation groundwater heat pump system. The Izbash equation and a linearization method are employed to describe non-Darcian flow in the horizontal direction of a confined aquifer and to approximate the nonlinear term in the governing equation, respectively. By applying a combination of the Laplace and Fourier cosine transforms, an approximate analytical solution in the Laplace domain is obtained, which is numerically inverted to obtain transient drawdown in the time domain using the Stehfest algorithm method. The results of the derived analytical solution for the special case of Darcian flow ($m = 1$) correspond well with the existing solution derived using Darcy's law. The steady-state analytical solution in the time domain is obtained by applying the Fourier cosine transform. Moreover, the sensitivity analysis is performed to investigate the influence of selected parameters, such as the power index m, the radial hydraulic conductivity K_r, the aquifer specific storage S, and the length of the sealed section d_2, on drawdown. The results show that each parameter has its influence period on drawdown, and that drawdown is more sensitive to the power index m compared to other parameters.

1. Introduction

It is well known that Darcy's law, which defines a linear relationship between the fluid flux and the hydraulic gradient, has been commonly used to address groundwater flow problems in practical engineering applications. However, the fluid flow becomes non-Darcian when the fluid flux is smaller or larger than a specific flux interval (Wilkinson, 1955; Slepicka, 1961; Bear, 1972; Zoorabadi et al., 2015; Zhou et al., 2015). When the relationship between the fluid flux and the hydraulic gradient deviates from classical Darcy's law, the flow becomes non-Darcian. Under these circumstances, researchers point out that Darcy's law is not sufficient to describe groundwater flow (Miller and Low, 1963; Bear, 1972; Barker and Herbert, 1977; Sen, 1985). A variety of equations has been derived to characterize the relationship between the fluid flux and the hydraulic gradient for non-Darcian flow (Forchheimer, 1901; Izbash, 1931; Muskat, 1938; Rose, 1951; Escande, 1953). Generally, these equations can be divided into two categories: power functions and polynomial functions (Wen et al., 2013). The first category assumes that the fluid flux is a power function of the hydraulic gradient, while the second category states that the fluid flux can be described as a second-order polynomial function of the hydraulic gradient.

Among equations of these two categories, the Forchheimer and Izbash equations are widely applied to describe non-Darcian flow (e.g., Sen, 1989; Sen, 1990; Wen et al., 2008a,b; Moutsopoulos et al., 2009; Mathias and Todman, 2010; Yeh and Chang, 2013; Sedghi-Asl et al., 2014; Chen et al., 2015; Houben, 2015). Until now, a variety of (approximate or semi-) analytical solutions for non-Darcian flow toward a fully or partially penetrating well has been derived for these two equations. For instance, Sen (1989, 1990) presented an analytical solution, which takes into account the non-Darcian flow described using the Forchheimer law toward an infinitesimal well or a large diameter well. An approximate analytical solution considering the effect of non-Darcian flow, which is defined by the Forchheimer equation, was derived by Wu (2002). Moutsopoulos and Tsihrintzis (2005) pre-

* Corresponding author at: College of Geoscience and Surveying Engineering, China University of Mining and Technology, Beijing 100083, China.
E-mail addresses: tukun2014@163.com (K. Tu), wuq@cumtb.edu.cn (Q. Wu).

https://doi.org/10.1016/j.advwatres.2020.103740
Received 31 January 2020; Received in revised form 21 July 2020; Accepted 14 August 2020
Available online 18 August 2020

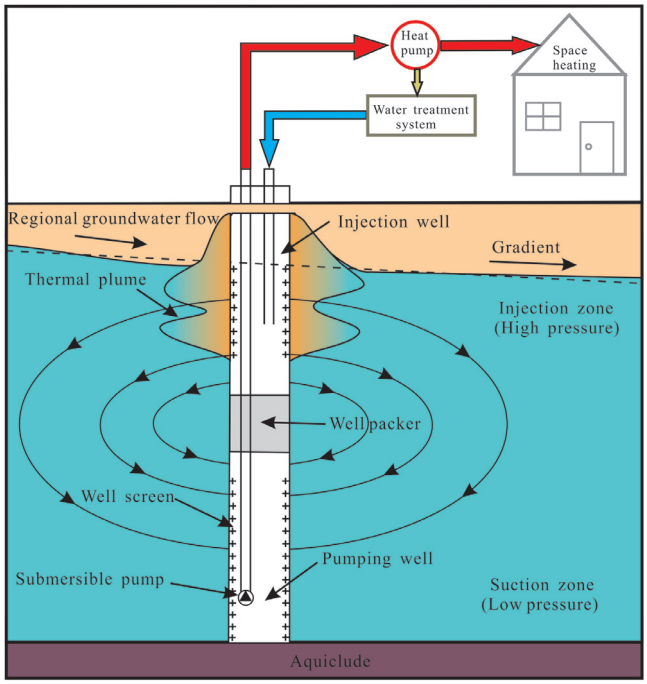

Fig. 1. A schematic of a single well circulation groundwater heat pump system (following Wu et al., 2019).

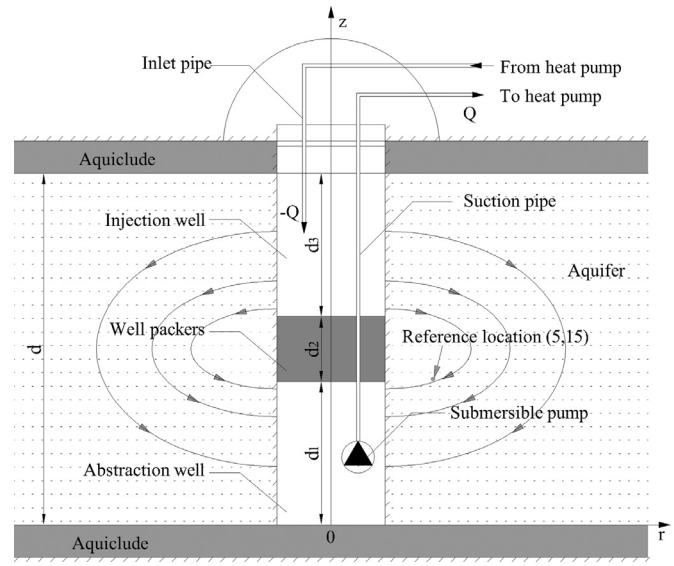

Fig. 2. The schematic diagram of the mathematical model for a single-well circulation system.

sented an approximate analytical solution for nonlinear flow through porous media described using the Forchheimer equation. Another approximate solution for Forchheimer's flow toward a well is presented by Mathias et al. (2008). Applying the Izbash equation, Sen (2000) provided an analytical solution for transient drawdown for non-Darcian flow to a fully penetrating well in a confined aquifer. Later, based on the Izbash equation, many efforts have been made by Wen et al. (2008) to develop analytical solutions describing non-Darcian flow towards a fully penetrating well. They presented several approximate analytical solutions in the Laplace domain, considering the effect of wellbore storage and a well radius in different aquifer systems. Furthermore, for non-Darcian flow toward a partially penetrating well, Wen et al. (2013) presented a semi-analytical solution in the Laplace domain while neglecting the effect of the well radius. They also investigated non-Darcian flow toward a larger diameter, partially penetrating well in a confined aquifer (Wen et al., 2014). An analytical solution describing non-Darcian flow to a partially penetrating well in a confined aquifer while considering the effect of a finite-thickness skin was presented by Feng and Wen (2016).

In addition to analytical solutions, numerical solutions for non-Darcian flow toward wells have also been developed. Wu (2002) employed the finite difference method to solve non-Darcian flow described using the Forchheimer equation through a fractured reservoir. Based on the assumption that the Forchheimer equation can describe non-Darcian flow, Mathias et al. (2008) investigated flow toward a fully penetrating well in a confined aquifer using the numerical model based on the finite difference method. Wen et al. (2009) developed a similar numerical model using the finite difference method and the assumption that the Izbash equation can be employed to describe the non-Darcian flow. Finally, Mathias and Wen (2015) performed a numerical simulation of non-Darcian flow in leaky aquifers using the Forchheimer equation.

A special well structure, referred to as a single well circulation system (Fig. 1), is commonly applied in practical engineering applications. In a single well circulation system, a single borehole is divided into two partially penetrating wells by well packers (as shown in Figs. 1 and 2), which are used to block water injected in the injection well to flow to the pumping well. The lower partially penetrating well is a pumping well with the pumping rate Q, and the upper partially penetrating well is an injection well for injecting water at the same rate Q. Thus, the single-well circulation system can be considered as a combination of two partially penetrating wells. To the best of our knowledge, little research work has been done on groundwater flow in a single well circulation system. Ni et al. (2011) presented an analytical solution describing the transient drawdown of groundwater induced by the operation of a single well circulation groundwater heat pump system. Subsequently, Tu et al. (2019) and Tu et al. (2020) developed an analytical solution describing the transient drawdown distribution and obtained a steady-state analytical solution in the time domain using the Laplace transform. It should be pointed out that these studies on groundwater flow in a single well circulation system are based on the assumption of Darcian flow.

However, because of very high hydraulic gradients and enhanced flow velocities due to the convergence of flow lines (Mathias et al., 2008; Yeh and Chang, 2013), a considerable number of researchers assumed that the flow in coarse-grained and fractured media near the wells likely becomes non-Darcian. The non-Darcian flow may also occur due to high fluxes near the wells, especially when the pumping/injection rates are relatively large (Wan et al., 2013; Wen et al., 2013; Wen et al., 2014; Feng and Wen, 2016). However, the research on groundwater flow in a single well circulation system has so far been based on the assumption of the validity of Darcy's law, which may not be adequate to describe the groundwater flow in such a system.

Practical engineering implementations of single well circulation groundwater heat pump systems require favorable aquifer conditions, which allow water flow at relatively high velocities to continuously provide a significant amount of water. The hydraulic conductivity of such aquifers should be at least 10^{-3}m/s or higher (Wu et al., 2015; Rybach, 2015). Besides, relatively large pumping rates (usually about 50–100 m^3/h; Rybach, 2015) are designed to meet the enormous energy demand. Therefore, the flow near the wells in a confined aquifer with a single well circulation system is particularly prone to become non-Darcian as a result of high flow velocities and hydraulic gradients.

To the best of our knowledge, most studies on non-Darcian flow have focused on systems with fully or partially penetrating wells (e.g., Wu, 2002; Mathias et al., 2008; Wen et al., 2008; Yeh and Chang, 2013; Wen et al., 2013; Mathias and Wen et al., 2015; Feng and Wen, 2016), while no analytical model has so far considered non-Darcian flow in a single well circulation system. It is, therefore, necessary to develop a new analytical model for investigating the effects of non-Darcian flow in a confined aquifer with a single well circulation system. This will

help in improving our understanding of the complex groundwater flow regime in single well circulation systems, which can be very beneficial for future investigations of heat convection in such systems.

The aim of this study is to extend the analytical solution based on Darcy's law to non-Darcian flow conditions and to investigate the effects of non-Darcian flow in a confined aquifer with a single well circulation system. This could have theoretical significance for the applications of single-well circulation groundwater heat pump systems. Due to relatively high pumping rates and large hydraulic conductivities in single well circulation systems, the horizontal flow velocity is usually very high, and non-Darcian flow near the wells likely occurs. The flow in the horizontal direction is, therefore, assumed to be non-Darcian. On the other hand, the flow velocity in the vertical direction is relatively small compared with the horizontal flow velocity. In order to make the analytical model tractable, the flow in the vertical direction is assumed to be Darcian. Such assumptions have been often adopted when dealing with non-Darcian flow problems and when the flow velocity in the vertical direction is considered (Wen et al., 2013; Wen et al., 2014; Feng and Wen, 2016).

The Izbash equation is used to describe non-Darcian flow, and a linearization approximation method proposed by Wen et al. (2008) is employed to solve the nonlinear term in the governing equation. This latter method has been shown to address this nonlinear problem efficiently. The approximate analytical solution in the Laplace domain is obtained by applying the Laplace and Fourier cosine transforms. The steady-state solution in the time domain is also developed using the linearization approximation method and the Fourier cosine transform. Moreover, sensitivity analysis is performed to investigate the influence of different parameters on drawdown.

2. Mathematical model

2.1. Model setup

Fig. 2 presents a schematic diagram that describes groundwater flow in a confined aquifer with a single-well circulation system. Non-Darcian flow is likely to occur because of the high flow velocity in the horizontal direction near the well, especially for a relatively large pumping rate. In this case, non-Darcian flow near the well needs to be considered. Due to a unique well structure, the flow in the vertical direction, which is assumed to be Darcian, cannot be neglected. Additional assumptions for this model are made: (1) the confined aquifer is treated as homogeneous and anisotropic with a uniform thickness d and infinite in the horizontal direction; (2) the underlying and overlying layers of the confined aquifer are both impermeable; (3) the specific discharge q_r in the horizontal direction is assumed to be constant along the screen (the same assumption as in Wen et al., 2013); (4) the pumping and injection rates Q (positive and negative values denote pumping and injection, respectively) are constant; and (5) the well radius r_w is infinitesimally small and can be neglected.

Based on the above descriptions and assumptions, the governing equation for the mathematical model can be written as follows:

$$\frac{\partial q_r}{\partial r} + \frac{q_r}{r} + \frac{\partial q_z}{\partial z} = S\frac{\partial s(r,z,t)}{\partial t} \tag{1}$$

where t is time [T], r and z represent the radial and vertical coordinates, respectively [L], S refers to the specific storage of an aquifer [L^{-1}], q_r and q_z denote the horizontal and vertical fluid fluxes, respectively [LT^{-1}], and s is groundwater drawdown [L].

Before the system starts functioning, groundwater drawdown is assumed to be zero, and the initial conditions for the system can be described as:

$$s(r,z,0) = 0 \tag{2}$$

The boundary conditions at infinity in the horizontal direction, $r = \infty$, and the bottom and top of a confined aquifer, $z = 0$ and $z = d$, are given as follows, respectively:

$$s(\infty,z,t) = 0 \tag{3}$$

and

$$\frac{\partial s(r,0,t)}{\partial z} = 0 \tag{4}$$

and

$$\frac{\partial s(r,d,t)}{\partial z} = 0 \tag{5}$$

where d is the thickness of a confined aquifer [L].

With the assumption that the wellbore storage is neglected, the boundary conditions near the well can be expressed as:

$$\lim_{r\to 0} rq_r = \begin{cases} \frac{-Q}{2\pi d_1} & (0 \le z \le d_1) \\ 0 & (d_1 \le z \le d_1 + d_2) \\ \frac{Q}{2\pi d_3} & (d_1 + d_2 \le z \le d) \end{cases} \tag{6}$$

where the pumping and injection rate Q (positive for pumping and negative for injection) are the same and constant [L^3T^{-1}]; d_1, d_2, and d_3 denote the lengths of well screens for pumping, sealed, and injection wells, respectively [L].

Izbash (1931) presented a power-law relationship between the hydraulic gradient and water flux, which can be employed to describe the non-Darcian flow. In this model, the horizontal specific discharge described by the Izbash equation for two-dimensional flow, same as in Wen et al. (2013), can be given as:

$$q_r|q_r|^{m-1} = K_r\frac{\partial s(r,z,t)}{\partial r} \tag{7}$$

where K_r is the (quasi) (Wen et al. 2006) radial hydraulic conductivity, and the non-Darcian exponent m in the Izbash's equation is an empirical coefficient that ranges between 1 and 2 and denotes the degree of deviation from linearity (Izbash, 1931; Bordier and Zimmer, 2000). When $m < 1$, the flow is treated as pre-linear flow, and when $1 < m \le 2$, the flow becomes post-linear flow (Izbash, 1931; Wen et al., 2006). It should be pointed out that Eq. (7) reduces to Darcy's law when $m = 1$.

Due to various factors, such as shapes and arrangements of pores, and complex flow paths, the non-Darcian exponent m varies in space and time (Bordier and Zimmer, 2000; Wen et al., 2006). It is thus quite difficult to determine and quantify its value in practical engineering applications. Although some researchers (Soni et al., 1978; Watanable, 1982; Chen et al., 2015) have attempted to determine the value of the non-Darcian exponent m, this issue has not yet been well resolved. In order to make the proposed models tractable, the non-Darcian exponent m is often assumed to be constant when dealing with non-Darcian flow problems (e.g., Sen, 2000; Wen et al., 2006, 2008; Quinn et al., 2011, 2013; Wen et al., 2013; Liu et al., 2016). However, adopting a constant non-Darcian exponent m in the Izbash's equation imposes some limitations when describing the non-Darcian flow. To overcome these limitations still remains an open issue and a very interesting topic for future investigations.

The flow in the vertical direction is assumed to be Darcian, which is described as:

$$q_z = K_z\frac{\partial s(r,z,t)}{\partial z} \tag{8}$$

where K_z represents the vertical hydraulic conductivity.

Since the flow in the horizontal direction is against the direction of the r coordinate, the specific discharge q_r is always negative. Thus, Eq. (7) can be furtherly reduced as:

$$(-q_r)^m = K_r\frac{\partial s(r,z,t)}{\partial r} \tag{9}$$

2.2. Approximate analytical solution

The governing equation of the mathematical model is obtained by substituting Eqs. (8) and (9) into Eq. (1):

$$\frac{K_r}{m(-q_r)^{m-1}}\frac{\partial^2 s(r,z,t)}{\partial r^2}+\frac{K_r}{r(-q_r)^{m-1}}\frac{\partial s(r,z,t)}{\partial r}+K_z\frac{\partial^2 s(r,z,t)}{\partial z^2}=S\frac{\partial s(r,z,t)}{\partial t} \tag{10}$$

It is noteworthy that Eq. (10) is a nonlinear equation due to the nonlinear term $(-q_r)^{m-1}$. Solving such a nonlinear equation may not be tractable using rigorous mathematical means. However, a linearization approximation method proposed by Wen et al. (2008) may be used to address this problem. This method has been successfully applied to find analytical solutions for other non-Darcian problems (e.g., Wen et al., 2008; Wen et al., 2013; Feng and Wen, 2016). By applying the linearization approximation method, the nonlinear term can be approximately described as:

$$(-q_r)^{m-1}\approx\left(\frac{Q}{2\pi rd}\right)^{m-1} \tag{11}$$

Substituting Eq. (11) into Eq. (10), one can obtain:

$$\frac{\partial^2 s(r,z,t)}{\partial r^2}+\frac{m}{r}\frac{\partial s(r,z,t)}{\partial r}+\frac{mK_z}{K_r}\left(\frac{Q}{2\pi rd}\right)^{m-1}\frac{\partial^2 s(r,z,t)}{\partial z^2}\approx\frac{mS}{K_r}\left(\frac{Q}{2\pi rd}\right)^{m-1}\frac{\partial s(r,z,t)}{\partial t} \tag{12}$$

Eq. (12) is a linear partial differential equation, which can be solved using the Laplace and Fourier cosine transforms. A detailed derivation of the solution of this partial differential equation can be seen in Appendix A. An approximate analytical solution of non-Darcian flow for the drawdown in the Laplace domain is given as:

$$\begin{aligned}\bar{s}(r,z,p)=&\frac{2\left(\frac{\sqrt{\alpha}}{3-m}\right)^{\frac{2}{3-m}}\left[\left(\frac{Q}{2\pi d_1}\right)^m d_1-\left(\frac{Q}{2\pi d_3}\right)^m d_3\right]}{pdK_r\sqrt{\alpha}\Gamma\left(\frac{2}{3-m}\right)}r^{\frac{1-m}{2}}K_{\frac{1-m}{3-m}}\left(\frac{2\sqrt{\alpha}}{3-m}r^{\frac{3-m}{2}}\right)\\&+\sum_{n=1}^{\infty}\frac{4\left(\frac{\sqrt{\varphi}}{3-m}\right)^{\frac{2}{3-m}}\left[\left(\frac{Q}{2\pi d_1}\right)^m sin\left(\frac{n\pi d_1}{d}\right)+\left(\frac{Q}{2\pi d_3}\right)^m sin\left(\frac{n\pi(d_1+d_2)}{d}\right)\right]}{n\pi pK_r\sqrt{\varphi}\Gamma\left(\frac{2}{3-m}\right)}r^{\frac{1-m}{2}}\\&\times K_{\frac{1-m}{3-m}}\left(\frac{2\sqrt{\varphi}}{3-m}r^{\frac{3-m}{2}}\right)cos\left(\frac{n\pi z}{d}\right)\end{aligned} \tag{13}$$

where $\varphi=\frac{mK_zn^2\pi^2+mpSd^2}{K_rd^2}(\frac{Q}{2\pi d})^{m-1}$, $\alpha=\frac{mpS}{K_r}(\frac{Q}{2\pi d})^{m-1}$; $\bar{s}$ is the solution of drawdown in the Laplace domain; $\Gamma(\cdot)$ denotes the gamma function; $K_v(\cdot)$ represents the modified Bessel function of the second kind with an order of v; and n and p are the Fourier and Laplace variables, respectively.

Due to the presence of the Bessel function $K_v(\cdot)$ term, it may not be possible to obtain the analytical solution of Eq. (13) in the time domain. However, several numerical inverse methods (e.g., Stehfest, 1970a,b; Crump, 1976; De Hoog et al., 1982) can be employed to transform the analytical solution in the Laplace domain to the time domain. In this work, an inverse Laplace transform is numerically conducted using the Stehfest method, which has been shown to address such inverse problems efficiently and accurately (Wen et al., 2008).

A program has been developed in MATLAB to calculate the solution for drawdown in the time domain based on the Stehfest method. The number of terms N, which are used in the inversion, needs to be specified before performing it. Multiple numerical studies have shown that the solution gives accurate and stable results with $N = 18$. Similarly, the infinite series of Eq. (13) converges when $n \geq 20$. Therefore, to increase computational efficiency, $N = 18$ and $n = 20$ are employed in the following calculations.

2.3. An analytical solution at a steady state

When the operation time of the system is long enough, the changes in drawdown near wells become stable, and the flow reaches steady-state conditions. In this case $\frac{\partial s(r,z,t)}{\partial t}=0$ and Eq. (12) becomes:

$$\frac{\partial^2 s(r,z)}{\partial r^2}+\frac{m}{r}\frac{\partial s(r,z)}{\partial r}+\frac{mK_z}{K_r}\left(\frac{Q}{2\pi rd}\right)^{m-1}\frac{\partial^2 s(r,z)}{\partial z^2}=0 \tag{14}$$

For this linear partial differential equation, the analytical solution at a steady state in the time domain is obtained by applying the Fourier cosine transform (see Appendix B):

$$\begin{aligned}(r,z)=&\frac{\left(\frac{Q}{2\pi d_1}\right)^m d_1-\left(\frac{Q}{2\pi d_3}\right)^m d_3}{dK_r\Gamma\left(\frac{2}{3-m}\right)(3-m)}r^{1-m}\\&+\sum_{n=1}^{\infty}\frac{4\left(\frac{\sqrt{\omega}}{3-m}\right)^{\frac{2}{3-m}}\left[\left(\frac{Q}{2\pi d_1}\right)^m sin\left(\frac{n\pi d_1}{d}\right)+\left(\frac{Q}{2\pi d_3}\right)^m sin\left(\frac{n\pi(d_1+d_2)}{d}\right)\right]}{n\pi K_r\sqrt{\omega}\Gamma\left(\frac{2}{3-m}\right)}\\&\times r^{\frac{1-m}{2}}K_{\frac{1-m}{3-m}}\left(\frac{2\sqrt{\omega}}{3-m}r^{\frac{3-m}{2}}\right)\cos\left(\frac{n\pi z}{d}\right)\end{aligned} \tag{15}$$

where $\omega=\frac{mK_z}{K_r}\frac{n^2\pi^2}{d^2}(\frac{Q}{2\pi d})^{m-1}$, and s is the drawdown in the time domain.

2.4. Simplification of the analytical solution

When $m = 1$, the flow becomes Darcian flow and the analytical solution of Eq. (13) is as follows:

$$\begin{aligned}\bar{s}(r,z,p)=&\sum_{n=1}^{\infty}\frac{Q}{npK_r\pi^2}\left[\frac{\sin\left(\frac{n\pi d_1}{d}\right)}{d_1}+\frac{\sin\left(\frac{n\pi(d_1+d_2)}{d}\right)}{d_3}\right]\\&\times K_0\left(\sqrt{\beta}r\right)\cos\left(\frac{n\pi z}{d}\right)\end{aligned} \tag{16}$$

where $\beta=\frac{K_z}{K_r}\frac{n^2\pi^2}{d^2}+\frac{pS}{K_r}$, and $K_0(\cdot)$ is the modified Bessel function of the second kind with an order of zero. The Eq. (16) is the same as the analytical solution derived by Tu et al. (2020) for Darcian flow in a confined aquifer with a single-well circulation system.

3. Results and discussion

3.1. Drawdown versus time as a function of the power index

The influence of the power index m (from 1 to 2) on drawdown observed at $r = 5$ m and $z = 15$ m is analyzed first when $Q = 60$ m^3/h, $d = 40$ m, $d_1 = 15$ m, $d_2 = 10$ m, $d_3 = 15$ m, $S = 0.0001$ m^{-1}, $K_r = 0.1$ (m/h)^m, and $K_z = 0.01$ m/h. For the case of $m = 1$ (Darcian flow), it can be observed in Fig. 3 that the drawdown calculated using the new analytical solution matches well the results of the analytical solution of Ni et al. (2011). The results in Fig. 3 indicate that the power index influences drawdown during the entire pumping period. A larger value of the power index results in larger drawdown at the beginning and smaller drawdown at later times (Fig. 3). A similar influence can also be found in Wen et al. (2013). A larger power index in the Izbash equation indicates more significant deviations from Darcian flow and results in greater flow turbulence. At early times, the elastic release process of an aquifer may be accelerated for a larger power index. Consequently, larger drawdown is observed at early times for a larger power index. As pumping time increases, drawdowns for different power indices approach a steady state when $t > 10$ h, indicating that the process of elastic release of an aquifer is approximately complete. Meanwhile, pumped water comes mainly from the region relatively far away from the pumping well. Larger flow turbulence induced by a larger power index is likely to result in larger

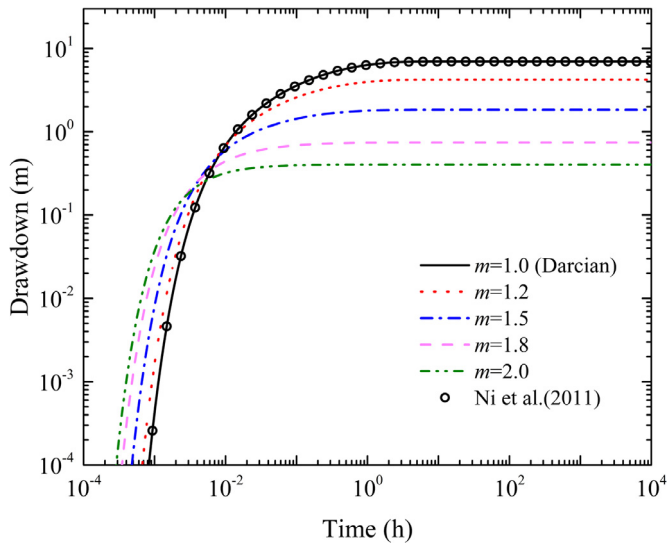

Fig. 3. The influence of the power index (m) on drawdown versus time.

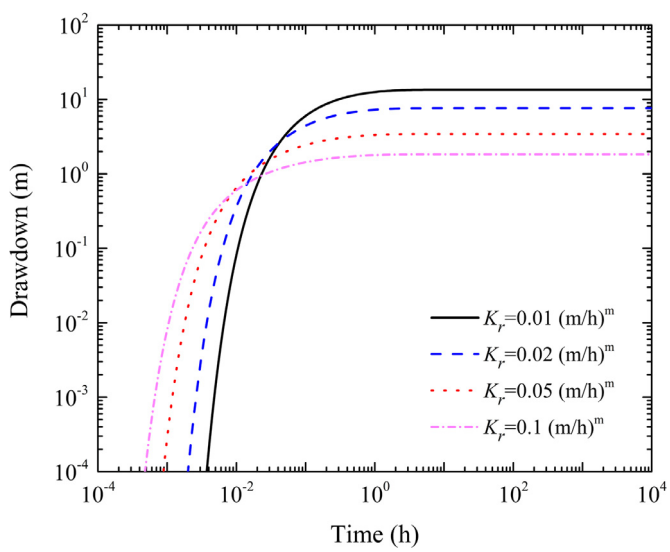

Fig. 4. The influence of the radial hydraulic conductivity (K_r) on drawdown versus time.

recharge. Therefore, it can be seen that drawdown is smaller for a larger power index at late times. Moreover, Fig. 3 also indicates that drawdown reaches a steady state more quickly when the power index is larger.

3.2. Drawdown versus time as a function of the radial hydraulic conductivity

Fig. 4 depicts temporal drawdown distribution curves observed at r = 5 m and z = 15 m for different radial hydraulic conductivities K_r from 0.01 to 0.1 m/h. Other parameters are as follows: Q = 60 m^3/h, m = 1.5, d = 40 m, d_1 = 15 m, d_2 = 10 m, d_3 = 15 m, S = 0.0001 m^{-1}, and K_z = 0.01 m/h. It is interesting to note that the influence of the radial hydraulic conductivity on drawdown is similar to that of the power index. As indicated in Fig. 4, drawdown increases with the radial hydraulic conductivity at the beginning, while smaller drawdown is obtained for larger radial hydraulic conductivities at late times. The reasons for this phenomenon can be explained as follows. At early times, larger hydraulic conductivities induce faster groundwater flow. Due to the faster spreading of the suction zone in the depression cone, groundwater can be replenished promptly. Consequently, larger drawdown for

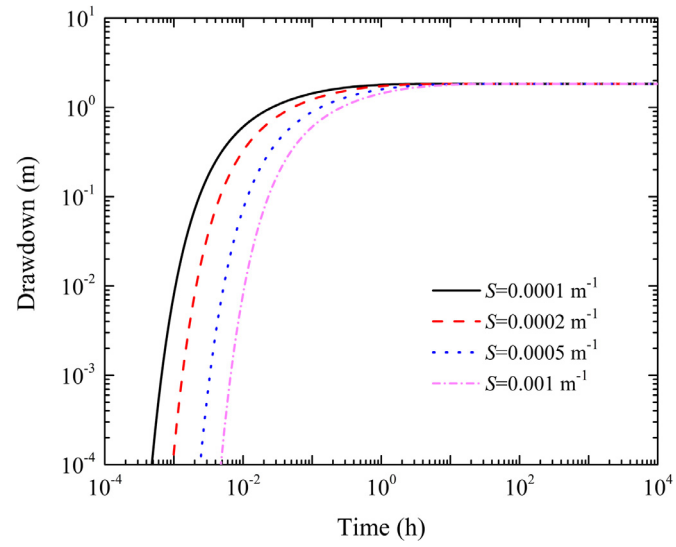

Fig. 5. The influence of the aquifer specific storage (S) on drawdown versus time.

a larger hydraulic conductivity at early times can be found. At late times, when the flow reaches a quasi-steady state, recharge occurs from areas relatively far away from the well. Smaller hydraulic conductivities will then result in a larger influence range of the depression cone and larger drawdown. Additionally, it is worth noting that drawdown approaches a steady state more quickly with increasing radial hydraulic conductivities (Fig. 4).

3.3. Drawdown versus time as a function of the aquifer specific storage

The curves in Fig. 5 show the temporal drawdown distributions observed at r = 5 m and z = 15 m calculated using the aquifer specific storage S from 0.0001 to 0.001 m^{-1}. The other parameters used to calculate the curves in the figure are as follows: Q = 60 m^3/h, m = 1.5, d = 40 m, d_1 = 15 m, d_2 = 10 m, d_3 = 15 m, K_r = 0.1 (m/h)^m, and K_z = 0.01 m/h. It is demonstrated in Fig. 5 that drawdown is smaller for a larger aquifer specific storage and vice versa at early times. A larger aquifer specific storage indicates that the aquifer can release more groundwater when other conditions remain the same. Moreover, at late times (t > 1 h), when the process of the storage release from the aquifer is almost complete, drawdown curves merge for different aquifer specific storages (Fig. 5). Drawdowns approach a steady state at late times, and the influence of different aquifer specific storages on drawdown is negligible.

3.4. Drawdown versus time as a function of the size of the sealed section

Fig. 6 shows drawdowns versus time observed at r = 5 m and z = 15 m for different lengths of the sealed section d_2 from 6 to 14 m. In this case, the thickness of the aquifer is kept constant, and the lengths of well screens for pumping and injection wells (d_1 and d_3, respectively) are correspondingly adjusted when the length of the sealed section changes. Other parameters used in this case are: Q = 60 m^3/h, m = 1.5, S = 0.0001 m^{-1}, K_r = 0.1 (m/h)^m, and K_z = 0.01 m/h. The curves shown in Fig. 6 indicate that changes in drawdown are significant when the length of the sealed section is reduced from 14 to 8 m. Also, larger lengths of the sealed section result in smaller drawdowns. Since the aquifer thickness and the pumping rate remain constant, the borehole with a longer length of the sealed section has a shorter length of the pumping screen and a correspondingly larger pumping rate for a unit length of the well screen. It is thus not surprising that larger drawdowns are obtained for shorter lengths of the sealed section. However, the influence of the further reduction in the length of the sealed section (from

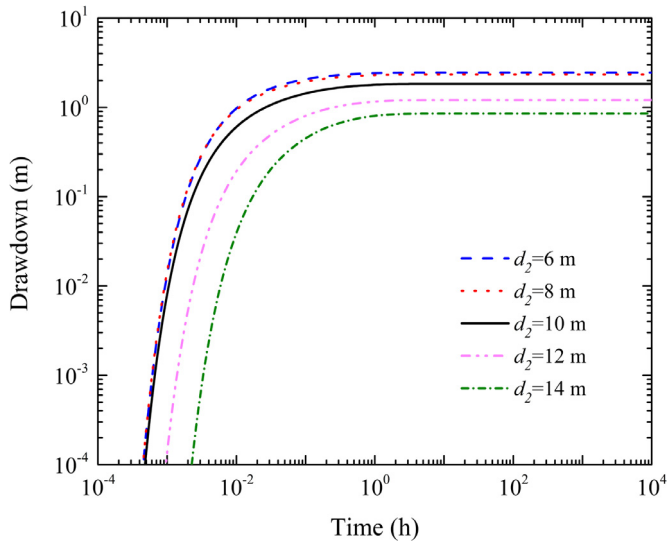

Fig. 6. The influence of the sealed section (d_2) on drawdown versus time.

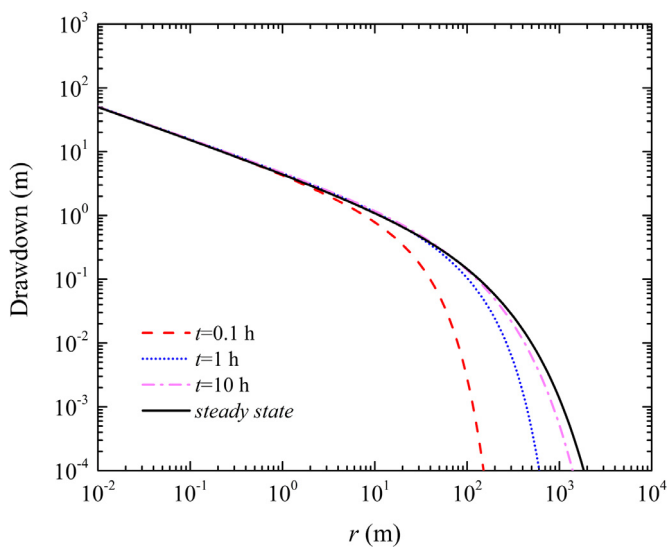

Fig. 7. The influence of the pumping time (t) on drawdown versus distance.

8 to 6 m) on drawdown is almost imperceptible. Also, differences in drawdown are smaller for smaller lengths of the sealed section (e.g., from 6 to 10 m) than for larger lengths of the sealed section. Moreover, when $t > 1$ h, drawdowns approach a steady state, and the curves are parallel.

3.5. Drawdown versus distance as a function of the pumping time

It is also important to analyze drawdown versus the radial distance for different pumping times (for $t = 0.1$, 1, 10 h, and at a steady state). The other parameters are as follows: $Q = 60$ m^3/h, $m = 1.5$, $d = 40$ m, $d_1 = 15$ m, $d_2 = 10$ m, $d_3 = 15$ m, $S = 0.0001$ m^{-1}, $K_r = 0.1$ (m/h)^m, and $K_z = 0.01$ m/h. The steady-state analytical solution, Eq. (15), is employed in this figure as a reference. It can be observed in Fig. 7 that drawdown curves merge for different pumping times when the radial distance $r < 1$ m, indicating that groundwater flow in the area around the pumping well reaches a steady state quickly. For the region further away from the well ($r > 1$ m), drawdown curves start deviating from each other. This is because the flow in this region is still unsteady and will take longer to reach a steady state. Moreover, drawdown at $t = 10$ h is very close to that at a steady state, which means that groundwater flow

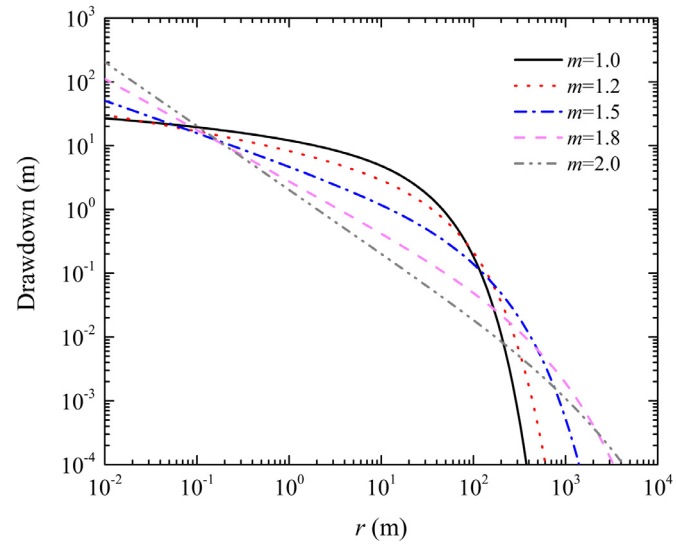

Fig. 8. The influence of the power index (m) on drawdown versus distance.

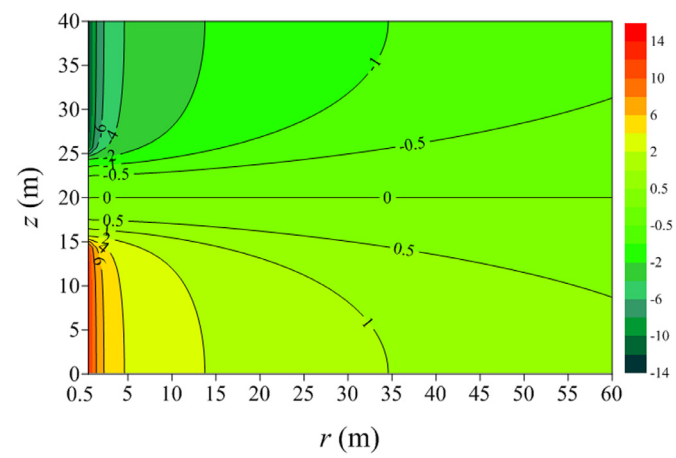

Fig. 9. Drawdown contours at a steady state.

in a confined aquifer for a single-well circulation system approaches a steady state relatively quickly.

3.6. Drawdown versus distance as a function of the power index

Temporal drawdown distribution curves versus a radial distance for different values of the power index m from 1 to 2 are shown in Fig. 8. The other parameters used in this figure are the same as before, i.e., $Q = 60$ m^3/h, $d = 40$ m, $d_1 = 15$ m, $d_2 = 10$ m, $d_3 = 15$ m, $t = 10$ h, $S = 0.0001$ m^{-1}, $K_r = 0.1$ (m/h)^m, and $K_z = 0.01$ m/h. It can be observed in Fig. 8 that a smaller value of the power index results in a larger drawdown for $r < 100$ m. However, at larger radial distances, drawdown for smaller values of the power index is smaller than for its larger values. This is consistent with the results in Fig. 3, implying that flow near the pumping well reached a steady state when the pumping time $t = 10$ h, while a steady state was not reached in the area far away from the pumping well (Fig. 8).

3.7. Drawdown contours at a steady state

Drawdown contours displayed in Fig. 9 are obtained using the analytical solution of Eq. (15) for steady-state conditions. The following parameters are used in this scenario: $Q = 60$ m^3/h, m = 1.5, $d = 40$ m, $d_1 = 15$ m, $d_2 = 10$ m, $d_3 = 15$ m, $S = 0.0001$ m^{-1}, $K_r = 0.1$ (m/h)^m,

Table 1
Ranges of parameters used in the global sensitivity analysis.

Uncertain parameter	Range
Power index m	1–2
Radial hydraulic conductivity K_r	0.01–0.1
Specific storage S	0.00001–0.0001
Length of the sealed section d_2	6–14

and $K_z = 0.01$ m/h. As shown in Fig. 7, changes in drawdown are very large for small r (less than 0.5 m), causing contours to be too dense to be displayed in Fig. 9. Therefore, the starting point on a horizontal axis in Fig. 9 is at $r = 0.5$ m. Due to flow symmetry, contours for steady-state drawdown are symmetric along a horizontal line at $z = 20$ m (the middle of a confined aquifer) where drawdown is equal to zero (Fig. 9) and vary tremendously along the well axis. When a single-well circulation system functions properly, pressure differences between the injection zone and the suction zone will yield relatively large hydraulic gradients near the wells. Thus, drawdown contours near the borehole are much denser than further away from the pumping or injection wells.

3.8. Sensitivity analysis

The global sensitivity analysis is an effective method that can be employed to analyze the sensitivity of the model output to changes in each input parameter (Saltelli et al., 2000). In particular, the Sobol's indices have been widely employed as sensitivity measures in many applications involving hydrological (van Werkhoven et al., 2009; Ciriello and Di Federico, 2012; Di Federico and Ciriello, 2012; Brunetti et al., 2016) and environmental (Nossent et al., 2011; Pianosi et al., 2015) models. This is because no assumptions of linearity or monotonicity are required for the adopted interpretative model (Sobol', 1993; Archer et al., 1997). These indices can provide accurate information about the model output variance related to a single parameter or associated with interactions of multiple parameters. A more detailed description of the Sobol' method can be found in Sobol' (2001).

According to the definition given by Sobol' (1993), the Sobol' sensitivity indices can be expressed as the ratio of the partial model variance to the total model variance:

$$\text{First-order } S_i = \frac{V_i}{V} \tag{17}$$

$$\text{Second-order } S_{ij} = \frac{V_{ij}}{V} \tag{18}$$

where V_i represents the partial variance of the model associated with the ith parameter, V_{ij} represents the partial variance of the model associated with the interaction of the ith and jth parameters, and V is the total variance. The first-order, or principal sensitivity, indices S_i, called the "main effect indices", are used to describe contributions of a single parameter to the total variance of the model output. The influence of the interaction of two input parameters on the model output variance is denoted as the second-order index, S_{ij}. The total sensitivity indices, S_{T_i} (Ciriello and Di Federico, 2012), represent the main effect of a given parameter (the ith parameter) and all its interactions with other parameters (up to the kth order, k denotes the number of input parameters), which can be expressed as follows:

$$\text{Total } S_{T_i} = S_i + \sum_{j \neq i} S_{ij} + \cdots \tag{19}$$

The evaluation of sensitivity indices is performed for the following parameters: the power index m, the radial hydraulic conductivity K_r, the aquifer specific storage S, and the length of the sealed section d_2. Table 1 shows the range of all evaluated parameters. Other conditions used when conducting the global sensitivity analysis are as follows: $Q = 60$ m^3/h, $d = 40$ m, $d_1 = d_3 = (40\text{-}d_2)/2$, and $K_z = 0.01$ m/h.

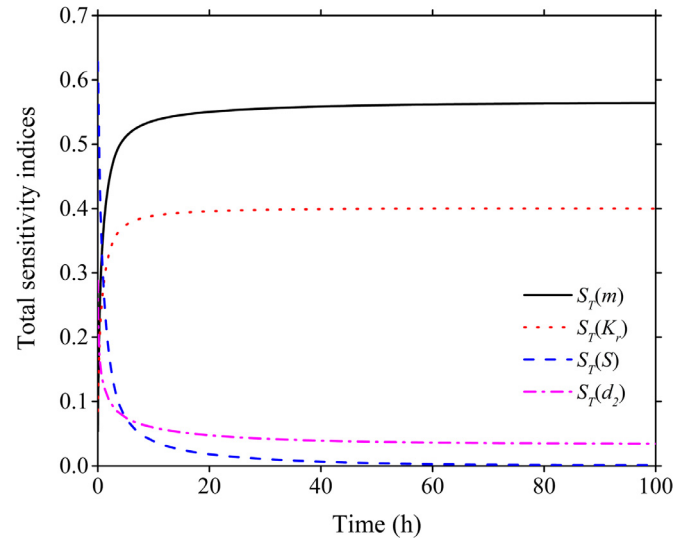

Fig. 10. The total sensitivity indices as a function of time for various parameters (the power index m, the aquifer specific storage S, the radial hydraulic conductivity K_r, and the length of the sealed section d_2).

Fig. 10 presents temporal changes in total sensitivity indices for selected input parameters. It can be seen that two parameters show a significant influence on the model output variance. These are the power index m and the radial hydraulic conductivity K_r. The total sensitivity index for the power index m is initially small, then increases with time, reaches a peak value near $t = 20$ h, and then remains constant with time. The radial hydraulic conductivity K_r shows a similar trend as the power index m, except that it has a lower peak value when reaching a steady state. The total sensitivity index for the specific storage S has initially a very high value, then sharply decreases until near $t = 10$ h, and then gradually drops to almost zero after $t > 40$ h. This indicates that the specific storage S has a negligible influence on the model output. Finally, the overall behavior of the total sensitivity index for the length of the sealed section d_2 is remarkably similar to that of the specific storage S, except that the total sensitivity indices reach a constant minimum value after large time, which is much larger compared with that for the specific storage S.

4. Conclusions

In this work, an analytical model has been developed to describe non-Darcian flow in a confined aquifer with a sing-well circulation system. Non-Darcian flow in the horizontal direction is described using the Izbash equation, and a linearization approach presented by Wen et al. (2008) is employed to approximate the nonlinear term in the governing equation. Then, using the Laplace and Fourier cosine transforms, the analytical solution in the Laplace domain is obtained, which is numerically inverted into the time domain using the Stehfest method. The main findings from this work can be drawn as follows:

(1) Larger values of the power index m and the radial hydraulic conductivity K_r result in larger drawdown at early times and smaller drawdown at late times. Groundwater flow approaches a steady state faster for larger values of the power index m and the radial hydraulic conductivity K_r.
(2) Larger values of the aquifer specific storage S result in smaller drawdown, while the influence of S on drawdown is negligible at late times.
(3) Smaller lengths of the sealed section d_2 result in larger drawdown. However, a further reduction in the length of the sealed section d_2 below a certain critical length leads to imperceptible changes in drawdown.

(4) The contours for steady-state drawdown vary significantly along the well axis and are symmetric around a horizontal line in the middle between the injection and suction sections ($z = 20$ m in our example) where drawdown is equal to zero.
(5) Each parameter has its influence period on drawdown. Drawdown is the most sensitive to the length of the sealed section d_2 and the aquifer specific storage S at early times, and the power index m (in particular) and the radial hydraulic conductivity K_r at late times.

Declaration of Competing Interest

We declare that we have no financial and personal relationships with other people or organizations that can inappropriately influence our work, there is no professional or other personal interest of any nature or kind in any product, service and/or company that could be construed as influencing the position presented in, or the review of, the manuscript entitled, "An approximate analytical solution for non-Darcian flow in a confined aquifer with a single well circulation groundwater heat pump system".

CRediT authorship contribution statement

Kun Tu: Conceptualization, Methodology, Writing - original draft, Software. **Qiang Wu:** Supervision, Project administration, Funding acquisition. **Jirka Simunek:** Supervision, Resources, Writing - review & editing. **Ke Zhu:** Methodology, Software. **Chaofan Chen:** Conceptualization, Formal analysis. **Weiyu Zheng:** Software, Formal analysis. **Yifan Zeng:** Conceptualization, Investigation. **Shengheng Xu:** Formal analysis.

Acknowledgments

The authors gratefully acknowledge the financial support from the Key Program of the National Natural Science Foundation of China (Grant No. 41430318), the National Scientific and Technical Support Program of China (Grant No. 2016YFC0801801), the National Natural Science Foundation of China (Grant No. 41572222, 41602262, 41702261), and the China Scholarship Council (No. 201806430053).

Appendix A. Derivation of the approximate analytical solution

The governing equation after applying the linearization method can be given as:

$$\frac{\partial^2 s(r,z,t)}{\partial r^2} + \frac{m}{r}\frac{\partial s(r,z,t)}{\partial r} + \frac{mK_z}{K_r}\left(\frac{Q}{2\pi rd}\right)^{m-1}\frac{\partial^2 s(r,z,t)}{\partial z^2} = \frac{mS}{K_r}\left(\frac{Q}{2\pi rd}\right)^{m-1}\frac{\partial s(r,z,t)}{\partial t} \tag{A1}$$

The Laplace transform with respect to time t is applied to Eq. (A1) to get:

$$\frac{\partial^2 \bar{s}(r,z,p)}{\partial r^2} + \frac{m}{r}\frac{\partial \bar{s}(r,z,p)}{\partial r} + \frac{mK_z}{K_r}\left(\frac{Q}{2\pi rd}\right)^{m-1}\frac{\partial^2 \bar{s}(r,z,p)}{\partial z^2} = \frac{mS}{K_r}\left(\frac{Q}{2\pi rd}\right)^{m-1} p\bar{s}(r,z,p) \tag{A2}$$

where p and $\bar{s}$ are the Laplace variable and drawdown in the Laplace domain, respectively.

Then, the Fourier cosine transform is used to the second-order partial derivative with respect to coordinate z in Eq. (A2) to obtain:

$$F_c\left[\frac{\partial^2 \bar{s}(r,z,p)}{\partial z^2}\right] = \int_0^d \frac{\partial^2 \bar{s}(r,z,p)}{\partial z^2} cos\left(\frac{n\pi z}{d}\right)dz = -\frac{n^2\pi^2}{d^2}\bar{\hat{s}}(r,n,p) \tag{A3}$$

where n ($n = 0, 1, 2, 3, \cdots\cdots$) is the Fourier variable, and $\bar{\hat{s}}(r,n,p)$ denotes the Fourier cosine transform of drawdown.

By substituting Eq. (A3) to Eq. (A2) we get:

$$\frac{d^2\bar{\hat{s}}(r,n,p)}{dr^2} + \frac{m}{r}\frac{d\bar{\hat{s}}(r,n,p)}{dr} = \frac{mK_z n^2\pi^2 + mpSd^2}{K_r d^2}\left(\frac{Q}{2\pi rd}\right)^{m-1}\bar{\hat{s}}(r,n,p) \tag{A4}$$

By defining $\varphi = \frac{mK_z n^2\pi^2 + mpSd^2}{K_r d^2}(\frac{Q}{2\pi d})^{m-1}$, Eq. (A4) can be reduced to:

$$\frac{d^2\bar{\hat{s}}(r,n,p)}{dr^2} + \frac{m}{r}\frac{d\bar{\hat{s}}(r,n,p)}{dr} - \varphi r^{1-m}\bar{\hat{s}}(r,n,p) = 0 \tag{A5}$$

Eq. (A5) is a linear differential equation of the second order. The general solution of Eq. (A5) can be described as:

$$\bar{\hat{s}}(r,n,p) = r^{\frac{1-m}{2}}\left[C_1 I_{\frac{1-m}{3-m}}\left(\frac{2\sqrt{\varphi}}{3-m}r^{\frac{3-m}{2}}\right) + C_2 K_{\frac{1-m}{3-m}}\left(\frac{2\sqrt{\varphi}}{3-m}r^{\frac{3-m}{2}}\right)\right] \tag{A6}$$

where $I_{\frac{1-m}{3-m}}(\cdot)$ and $K_{\frac{1-m}{3-m}}(\cdot)$ are the modified Bessel functions of the first and second kind with the order of $\frac{1-m}{3-m}$, respectively. The integration constants C_1 and C_2 can be determined according to boundary conditions.

By applying the Laplace and Fourier cosine transforms to Eq. (3) one can obtain:

$$\bar{\hat{s}}(\infty,n,p) = 0 \tag{A7}$$

Considering the property of the modified Bessel function of the first kind and substituting Eq. (A7) to Eq. (A6) one gets:

$$C_1 = 0 \tag{A8}$$

Eq. (A6) can then be rewritten as:

$$\bar{\hat{s}}(r,n,p) = C_2 r^{\frac{1-m}{2}} K_{\frac{1-m}{3-m}}\left(\frac{2\sqrt{\varphi}}{3-m}r^{\frac{3-m}{2}}\right) \tag{A9}$$

Combining the Izbash equation and the linearization method, the boundary conditions of Eq. (6) can be given as:

$$\lim_{r\to 0}\frac{\partial s(r,z,t)}{\partial r} = \begin{cases} -\frac{1}{K_r}\left(\frac{Q}{2\pi rd_1}\right)^m & (0 \le z \le d_1) \\ 0 & (d_1 \le z \le d_1 + d_2) \\ \frac{1}{K_r}\left(\frac{Q}{2\pi rd_3}\right)^m & (d_1 + d_2 \le z \le d) \end{cases} \tag{A10}$$

Applying the Laplace and Fourier cosine transforms to Eq. (A10), one can obtain:

$$\lim_{r\to 0}\frac{d\bar{\hat{s}}(r,n,p)}{dr} = \lim_{r\to 0}\frac{-d}{n\pi pK_r}\left[\left(\frac{Q}{2\pi rd_1}\right)^m sin\left(\frac{n\pi d_1}{d}\right) + \left(\frac{Q}{2\pi rd_3}\right)^m sin\left(\frac{n\pi(d_1+d_2)}{d}\right)\right] \tag{A11}$$

The modified Bessel function has the following properties (Spanier and Oldham, 1987):

$$\frac{xdK_v(x)}{dx} + vK_v(x) = -xK_{v-1}(x) \tag{A12}$$

and

$$K_v(x) = K_{-v}(x) \tag{A13}$$

and

$$K_v(x) \approx \frac{\Gamma(v)}{2}\left(\frac{x}{2}\right)^{-v},\ x \to 0,\ v > 0 \tag{A14}$$

From Eqs. (A9), (A12), (A13), and (A14), one has:

$$\lim_{r\to 0}\frac{d\bar{\hat{s}}(r,n,p)}{dr} = -\frac{1}{2}\lim_{r\to 0}C_2\frac{1}{r^m}\sqrt{\varphi}\Gamma\left(\frac{2}{3-m}\right)\left(\frac{\sqrt{\varphi}}{3-m}\right)^{-\frac{2}{3-m}} \tag{A15}$$

The integration constant C_2 can then be obtained from Eqs. (A11) and (A15) as:

$$C_2 = \frac{2d\left(\frac{\sqrt{\varphi}}{3-m}\right)^{\frac{2}{3-m}}\left[\left(\frac{Q}{2\pi d_1}\right)^m sin\left(\frac{n\pi d_1}{d}\right)+\left(\frac{Q}{2\pi d_3}\right)^m sin\left(\frac{n\pi(d_1+d_2)}{d}\right)\right]}{n\pi p K_r\sqrt{\varphi}\Gamma\left(\frac{2}{3-m}\right)} \tag{A16}$$

Substituting Eq. (A16) to Eq. (A9), one gets:

$$\bar{\hat{s}}(r,n,p) = \frac{2d\left(\frac{\sqrt{\varphi}}{3-m}\right)^{\frac{2}{3-m}}\left[\left(\frac{Q}{2\pi d_1}\right)^m sin\left(\frac{n\pi d_1}{d}\right)+\left(\frac{Q}{2\pi d_3}\right)^m sin\left(\frac{n\pi(d_1+d_2)}{d}\right)\right]}{n\pi p K_r\sqrt{\varphi}\Gamma\left(\frac{2}{3-m}\right)} \times r^{\frac{1-m}{2}} K_{\frac{1-m}{3-m}}\left(\frac{2\sqrt{\varphi}}{3-m} r^{\frac{3-m}{2}}\right) \tag{A17}$$

When the inverse Fourier transform is employed to Eq. (17), one can obtain:

$$\bar{s}(r,z,p) = \frac{1}{d}\bar{\hat{s}}(r,0,p) + \frac{2}{d}\sum_{n=1}^{\infty}\bar{\hat{s}}(r,n,p)cos\left(\frac{n\pi z}{d}\right) \tag{A18}$$

When $n = 0$, similar processes are applied to solve Eq. (A5) and boundary conditions, and finally the integration constant C_2' can be obtained as:

$$C_2' = \frac{2\left(\frac{\sqrt{\alpha}}{3-m}\right)^{\frac{2}{3-m}}\left[\left(\frac{Q}{2\pi d_1}\right)^m d_1 - \left(\frac{Q}{2\pi d_3}\right)^m d_3\right]}{pK_r\sqrt{\alpha}\Gamma\left(\frac{2}{3-m}\right)} \tag{A19}$$

where $\alpha = \frac{mpS}{K_r}(\frac{Q}{2\pi d})^{m-1}$. Then, with Eq. (A19), one has:

$$\bar{\hat{s}}(r,0,p) = \frac{2\left(\frac{\sqrt{\alpha}}{3-m}\right)^{\frac{2}{3-m}}\left[\left(\frac{Q}{2\pi d_1}\right)^m d_1 - \left(\frac{Q}{2\pi d_3}\right)^m d_3\right]}{pK_r\sqrt{\alpha}\Gamma\left(\frac{2}{3-m}\right)} r^{\frac{1-m}{2}} K_{\frac{1-m}{3-m}}\left(\frac{2\sqrt{\alpha}}{3-m} r^{\frac{3-m}{2}}\right) \tag{A20}$$

Finally, the analytical solution in the Laplace domain can be obtained by substituting Eqs. (A17) and (A20) to Eq. (A18).

Appendix B. Derivation of the steady-state analytical solution

Similarly, the Fourier cosine transform is used to the second-order partial derivative with respect to coordinate z in Eq. (14) to get:

$$F_c\left[\frac{\partial^2 s(r,z)}{\partial z^2}\right] = \int_0^d \frac{\partial^2 s(r,z)}{\partial z^2} cos\left(\frac{n\pi z}{d}\right)dz = -\frac{n^2\pi^2}{d^2}\hat{s}(r,n) \tag{B1}$$

where $\hat{s}$ is drawdown in the Fourier domain.

By applying the Fourier cosine transform to Eq. (14) and combining it with Eq. (B1), Eq. (14) can then be reduced to:

$$\frac{d^2\hat{s}(r,n)}{dr} + \frac{m}{r}\frac{d\hat{s}(r,n)}{dr} - \omega r^{1-m}\hat{s}(r,n) = 0 \tag{B2}$$

in which $\omega = \frac{mK_z}{K_r}\frac{n^2\pi^2}{d^2}(\frac{Q}{2\pi d})^{m-1}$. The general solution of Eq. (B2) is obtained as:

$$\hat{s}(r,n) = r^{\frac{1-m}{2}}\left[C_3 I_{\frac{1-m}{3-m}}\left(\frac{2\sqrt{\omega}}{3-m} r^{\frac{3-m}{2}}\right) + C_4 K_{\frac{1-m}{3-m}}\left(\frac{2\sqrt{\omega}}{3-m} r^{\frac{3-m}{2}}\right)\right] \tag{B3}$$

where C_3 and C_4 are integration constants; $I_{\frac{1-m}{3-m}}(\cdot)$ and $K_{\frac{1-m}{3-m}}(\cdot)$ denote the modified Bessel functions of the first and second kind with the order of $\frac{1-m}{3-m}$, respectively. Using the boundary condition Eq. (3), the constant C_3 can be obtained by applying the Fourier transform and properties of the modified Bessel function, leading to $C_3 = 0$. Then, Eq. (B3) can be further written as:

$$\hat{s}(r,n) = C_4 r^{\frac{1-m}{2}} K_{\frac{1-m}{3-m}}\left(\frac{2\sqrt{\omega}}{3-m} r^{\frac{3-m}{2}}\right) \tag{B4}$$

Using the Fourier cosine transform to Eq. (6), one can obtain:

$$\lim_{r\to 0}\frac{d\hat{s}(r,n)}{dr} = \lim_{r\to 0}\frac{-d}{n\pi K_r}\left[\left(\frac{Q}{2\pi r d_1}\right)^m sin\left(\frac{n\pi d_1}{d}\right) + \left(\frac{Q}{2\pi r d_3}\right)^m sin\left(\frac{n\pi(d_1+d_2)}{d}\right)\right] \tag{B5}$$

With Eq. (B4) and the properties of the modified Bessel function as described in Eqs. (A12), (A13), and (A14), one has:

$$\lim_{r\to 0}\frac{d\hat{s}(r,n)}{dr} = -\frac{1}{2}\lim_{r\to 0} C_4\frac{1}{r^m}\sqrt{\omega}\Gamma\left(\frac{2}{3-m}\right)\left(\frac{\sqrt{\omega}}{3-m}\right)^{\frac{-2}{3-m}} \tag{B6}$$

Combining Eqs. (B5) and (B6), the constant C_4 can be given as:

$$C_4 = \frac{2d\left(\frac{\sqrt{\omega}}{3-m}\right)^{\frac{2}{3-m}}\left[\left(\frac{Q}{2\pi d_1}\right)^m sin\left(\frac{n\pi d_1}{d}\right)+\left(\frac{Q}{2\pi d_3}\right)^m sin\left(\frac{n\pi(d_1+d_2)}{d}\right)\right]}{n\pi K_r\sqrt{\omega}\Gamma\left(\frac{2}{3-m}\right)} \tag{B7}$$

Substituting Eq. (B7) to Eq. (B4), one can obtain:

$$\hat{s}(r,n) = \frac{2d\left(\frac{\sqrt{\omega}}{3-m}\right)^{\frac{2}{3-m}}\left[\left(\frac{Q}{2\pi d_1}\right)^m sin\left(\frac{n\pi d_1}{d}\right)+\left(\frac{Q}{2\pi d_3}\right)^m sin\left(\frac{n\pi(d_1+d_2)}{d}\right)\right]}{n\pi K_r\sqrt{\omega}\Gamma\left(\frac{2}{3-m}\right)} \times r^{\frac{1-m}{2}} K_{\frac{1-m}{3-m}}\left(\frac{2\sqrt{\omega}}{3-m} r^{\frac{3-m}{2}}\right) \tag{B8}$$

Applying the inverse of Fourier cosine transform to Eq. (B8), one has:

$$s(r,z) = \frac{1}{d}\hat{s}(r,0) + \frac{2}{d}\sum_{n=1}^{\infty}\hat{s}(r,n)\cos\left(\frac{n\pi z}{d}\right) \tag{B9}$$

When $n = 0$, Eq. (B2) with corresponding boundary conditions can be solved using similar methods. Then, using properties of the modified Bessel function from Eq. (A12) to Eq. (A14), the term $\hat{s}(r,0)$ in Eq. (B9) can be obtained as:

$$\hat{s}(r,0) = \frac{\left(\frac{Q}{2\pi d_1}\right)^m d_1 - \left(\frac{Q}{2\pi d_3}\right)^m d_3}{K_r\Gamma\left(\frac{2}{3-m}\right)(3-m)} r^{1-m} \tag{B10}$$

Substituting Eqs. (B8) and (B10) to Eq. (B9), we can eventually obtain the steady-state analytical solution in the time domain.

References

Archer, G.E.B., Saltelli, A., Sobol, I.M., 1997. Sensitivity measures, ANOVA-like techniques and the use of bootstrap. J. Statist. Comput. Simulation 58 (2), 99–120.

Barker, J.A., Herbert, R., 1977. Non-Darcy flow and its implications to seepage problem. J. Irrig. Drain. Eng.-ASCE 459–473.

Bear, J., 1972. Dynamics of Fluid in Porous Media. Elsevier Science, New York.

Bordier, Zimmer, 2000. Drainage equations and non-Darcian modelling in coarse porous media or geosynthetic materials. Journal of Hydrology.

Brunetti, G., Šimůnek, J., Piro, P., 2016. A comprehensive numerical analysis of the hydraulic behavior of a permeable pavement. J. Hydrol. 540, 1146–1161.

Chen, Y.F., Hu, S.H., Hu, R., Zhou, C.B., 2015. Estimating hydraulic conductivity of fractured rocks from high-pressure packer tests with an Izbash's law-based empirical model. Water Resour. Res. 51 (4), 2096–2118.

Chen, Y.F., Liu, M.M., Hu, S.H., Zhou, C.B., 2015. Non-Darcy's law-based analytical models for data interpretation of high-pressure packer tests in fractured rocks. Eng. Geol. 199, 91–106.

Ciriello, V., Di Federico, V., 2012. Similarity solutions for flow of non-Newtonian fluids in porous media revisited under parameter uncertainty. Adv. Water Res. 43, 38–51.

Crump, K.S., 1976. Numerical inversion of Laplace transforms using a Fourier-series approximation. J. ACM (JACM) 23 (1), 89–96.

De Hoog, F.R., Knight, J.H., Stokes, A.N., 1982. An improved method for numerical inversion of Laplace transforms. SIAM J. Sci. Stat. Comput. 3 (3), 357–366.
Di Federico, V., Ciriello, V., 2012. Generalized solution for 1-D non-Newtonian flow in a porous domain due to an instantaneous mass injection. Transp. Porous Media 93 (1), 63–77.
Escande, L., 1953. Experiments concerning the filtration of water through rock mass. Proceeding of Minnesota International Hydraulics Convention.
Feng, Q., Wen, Z., 2016. Non-Darcian flow to a partially penetrating well in a confined aquifer with a finite-thickness skin. Hydrogeol. J. 24 (5), 1287–1296.
Forchhelmer, P.H., 1901. Wasserbewegun durch boden. Zeltschrlft des Verelnes Deutscher Ingenleure 49, 1736–1749.
Houben, G.J., 2015. Hydraulics of water wells-flow laws and influence of geometry. Hydrogeol. J. 23 (8), 1633–1657.
Izbash, S.V., 1931. O filtracii v kropnozernstom materiale. USSR, Leningrad in Russian.
Liu, M.M., Chen, Y.F., Hong, J.M., Zhou, C.B., 2016. A generalized non-Darcian radial flow model for constant rate test. Water Resour. Res. 52 (12), 9325–9343.
Mathias, S.A., Butler, A.P., Zhan, H., 2008. Approximate solutions for Forchheimer flow to a well. J. Hydraul. Eng. 134 (9), 1318–1325.
Mathias, S.A., Todman, L.C., 2010. Step-drawdown tests and the Forchheimer equation. Water Resour. Res. 46 (7).
Mathias, S.A., Butler, A.P., Zhan, H.B., 2008. Approximate solutions for Forchheimer flow to a well. J. Hydraul. Eng. 134 (9), 1318–1325.
Mathias, S.A., Wen, Z., 2015. Numerical simulation of Forchheimer flow to a partially penetrating well with a mixed-type boundary condition. J. Hydrol. 524, 53–61.
Miller, R.J., Low, P.F., 1963. Threshold gradient for water flow in clay systems. Soil Sci. Soc. Am. J. 27 (6), 605–609.
Moutsopoulos, K.N., Papaspyros, I.N., Tsihrintzis, V.A., 2009. Experimental investigation of inertial flow processes in porous media. J. Hydrol. 374, 242–254.
Moutsopoulos, K.N., Tsihrintzis, V.A., 2005. Approximate analytical solutions of the Forchheimer equation. J. Hydrol. 309 (1–4), 93–103.
Muskat, M., 1938. The flow of homogeneous fluids through porous media. Soil Sci. 46 (2), 169.
Ni, L., Li, H., Jiang, Y., Yao, Y., Ma, Z., 2011. A model of groundwater seepage and heat transfer for single-well ground source heat pump systems. Appl. Therm. Eng. 31, 2622–2630.
Nossent, J., Elsen, P., Bauwens, W., 2011. Sobol' sensitivity analysis of a complex environmental model. Environ. Model. Softw. 26 (12), 1515–1525.
Pianosi, F., Sarrazin, F., Wagener, T., 2015. A Matlab toolbox for global sensitivity analysis. Environ. Model. Softw. 70, 80–85.
Quinn, P.M., Cherry, J.A., Parker, B.L., 2011. Quantification of non-Darcian flow observed during packer testing in fractured sedimentary rock. Water Resour. Res. 47 (9).
Quinn, P.M., Parker, B.L., Cherry, J.A., 2013. Validation of non-Darcian flow effects in slug tests conducted in fractured rock boreholes. J. Hydrol. 486, 505–518.
Rose, H.E., 1951. Fluid flow through beds of granular material. In: Some Aspects of Fluid Flow. Edward Arnold, London, pp. 136–163.
Rybach, L., 2015. Innovative energy-related use of shallow and deep groundwaters-examples from China and Switzerland. Cent. Eur. Geol. 58 (1–2), 100–113.
Saltelli, A., Chan, K., Scott, E.M., 2000. *Sensitivity Analysis*. Wiley, New York, USA.
Sedghi-Asl, M., Rahimi, H., Salehi, R., 2014. Non-Darcy flow of water through a packed column test. Transp. Porous Media 101 (2), 215–227.
Sen, Z., 1985. Volumetric approach to type curves in leaky aquifers. J. Hydraul. Eng. 111 (3), 467–484.
Sen, Z., 1989. Nonlinear flow toward wells. J. Hydraul. Eng. 115 (2), 193–209.
Şen, Z., 1990. Nonlinear radial flow in confined aquifers toward large-diameter wells. Water Resour. Res. 26 (5), 1103–1109.
Sen, Z., 2000. Non-Darcian groundwater flow in leaky aquifers. Hydrol. Sci. J. 45 (4), 595–606.
Slepicka, F., 1961. The laws of filtration and limits of their validity. In: IAHR Proceedings 9th Convention, 38, pp. 383–394.
Sobol, I.M., 1993. Sensitivity estimates for nonlinear mathematical models. Math. Model. Comput. Exp. 1 (4), 407–414.
Sobol, I.M., 2001. Global sensitivity indices for nonlinear mathematical models and their Monte Carlo estimates. Math. Comput. Simul 55 (1–3), 271–280.
Soni, J.P., Islam, N., Basak, P., 1978. An experimental evaluation of non-Darcian flow in porous media. J. Hydrol. 38 (3–4), 231–241.
Spanier, J., Oldham, K.B., 1987. An Atlas of Functions. Hemisphere, New York, USA.
Stehfest, H., 1970a. Algorithm 368: Numerical inversion of Laplace transforms [D5]. Commun. ACM 13 (1), 47–49.
Stehfest, H., 1970b. Remark on algorithm 368: numerical inversion of Laplace transforms [D5]. Commun. ACM 13 (10), 624–625.
Tu, K., Wu, Q., Simunek, J., Chen, C., Zhu, K., Zeng, Y., Xu, S., Wang, Y., 2020. An analytical solution of groundwater flow in a confined aquifer with a single well circulation system. Water Resour. Res. 56 e2020WR027529.
Tu, K., Wu, Q., Sun, H., 2019. A mathematical model and thermal performance analysis of single-well circulation (SWC) coupled ground source heat pump (GSHP) systems. Appl. Therm. Eng. 147, 473–481.
Watanabe, H., 1982. Comment on Izbash's equation. J. Hydrol. 58 (3–4), 389–397.
van Werkhoven, K., Wagener, T., Reed, P., Tang, Y., 2009. Sensitivity-guided reduction of parametric dimensionality for multi-objective calibration of watershed models. Adv. Water Res. 32 (8), 1154–1169.
Wan, J.W., Huang, K., Chen, C.X., 2013. Reassessing Darcy'Law on water flow in porous media. Earth Sci.-J. China Univ. Geosci. 38 (6), 1327–1330 in Chinese.
Wen, Z., Huang, G., Zhan, H., 2006. Non-Darcian flow in a single confined vertical fracture toward a well. J. Hydrol. 330, 698–708.
Wen, Z., Huang, G., Zhan, H., 2008. An analytical solution for non-Darcian flow in a confined aquifer using the power law function. Adv. Water Res. 31 (1), 44–55.
Wen, Z., Huang, G., Zhan, H., 2008b. Non-Darcian flow to a well in an aquifer–aquitard system. Adv. Water Res. 31 (12), 1754–1763.
Wen, Z., Huang, G., Zhan, H., 2009. A numerical solution for non-Darcian flow to a well in a confined aquifer using the power law function. J. Hydrol. 364 (1–2), 99–106.
Wen, Z., Huang, G., Zhan, H., Li, J., 2008a. Two-region non-Darcian flow toward a well in a confined aquifer. Adv. Water Res. 31 (5), 818–827.
Wen, Z., Liu, K., Chen, X., 2013. Approximate analytical solution for non-Darcian flow toward a partially penetrating well in a confined aquifer. J. Hydrol. 498, 124–131.
Wen, Z., Liu, K., Zhan, H., 2014. Non-Darcian flow toward a larger-diameter partially penetrating well in a confined aquifer. Environ. Earth Sci. 72 (11), 4617–4625.
Wilkinson, J.K., 1955. Flow of water through rock fill and its application to the design of dams. N.Z. Eng. 10 (11), 382–387.
Wu, Q., Tu, K., Sun, H., Chen, C., 2019. Investigation on the sustainability and efficiency of single-well circulation (SWC) groundwater heat pump systems. Renew. Energy 130, 656–666.
Wu, Q., Xu, S.H., Zhou, W.F., LaMoreaux, J., 2015. Hydrogeology and design of groundwater heat pump systems. Environ. Earth Sci. 73 (7), 3683–3695.
Wu, Y.S., 2002. An approximate analytical solution for non-Darcy flow toward a well in fractured media. Water Resour. Res. 38 (3) 5–1.
Yeh, H.D., Chang, Y.C., 2013. Recent advances in modeling of well hydraulics. Adv. Water Res. 51, 27–51.
Zhou, J.Q., Hu, S.H., Fang, S., Chen, Y.F., Zhou, C.B., 2015. Nonlinear flow behavior at low Reynolds numbers through rough-walled fractures subjected to normal compressive loading. Int. J. Rock Mech. Min. Sci. 80, 202–218.
Zoorabadi, M., Saydam, S., Timms, W., Hebblewhite, B., 2015. Nonlinear flow behavior of rough fractures having standard JRC profiles. Int. J. Rock Mech. Min. 76, 192–199.